



1

2 **Can label or protein deuteration extend the phase relaxation time of Gd(III) spin labels?**

3 Elena Edinach<sup>1#</sup>, Xing Zhang<sup>2#</sup>, Chao-Yu Cui<sup>2</sup>, Yin Yang<sup>2</sup>, George Mitrikas<sup>3</sup>, Alexey Bogdanov<sup>1</sup>, Xun-  
4 Cheng Su<sup>2,\*</sup>, and Daniella Goldfarb<sup>1,\*</sup>

5 <sup>1</sup>Department of Chemical and Biological Physics, Weizmann Institute of Science, 76100 Rehovot,  
6 Israel

7 <sup>2</sup>State Key Laboratory of Elemento-Organic Chemistry, College of Chemistry, Nankai University,  
8 300071 Tianjin, China

9 <sup>3</sup>Institute of Nanoscience and Nanotechnology, NCSR Demokritos, Athens 15310, Greece

10

11 Corresponding authors : Xun-Cheng Su, [xunchengsu@nankai.edu.cn](mailto:xunchengsu@nankai.edu.cn), Daniella Goldfarb,  
12 [Daniella.goldfarb@weizmann.ac.il](mailto:Daniella.goldfarb@weizmann.ac.il)

13

14 <sup>#</sup>Equal contributions

15



## 1 Abstract

2 Pulse-dipolar electron paramagnetic resonance (PD-EPR) has emerged as an effective tool in  
3 structural biology, enabling distance measurements between spin labels attached to  
4 biomolecules. The sensitivity and the accessible distance range of these measurements are  
5 governed by the phase memory time ( $T_m$ ) of the spin labels. Understanding the decoherence  
6 mechanisms affecting  $T_m$  is crucial for optimizing sample preparation and spin-label design. This  
7 study investigates the phase relaxation behavior of two Gd(III) spin-label complexes, Gd-PyMTA  
8 and Gd-TPMTA, with various degrees of deuteration. These two complexes have significantly  
9 different zero-field splitting (ZFS) parameters. Hahn echo decay and dynamical decoupling (DD)  
10 measurements were performed at W-band (95 GHz) in deuterated solvents ( $D_2O$ /glycerol- $d_8$ ),  
11 both for the free complexes and when conjugated to proteins. The impact of temperature,  
12 concentration, and field position within the EPR spectrum on  $T_m$  was examined. Results indicate  
13 that protons within 5 Å of the Gd(III) ion do not contribute to nuclear spin diffusion (NSD), and  
14 protein deuteration offers minimal enhancement in  $T_m$ . The dominant phase relaxation  
15 mechanisms identified at low concentrations were direct spin-lattice relaxation ( $T_1$ ) and  
16 transient ZFS fluctuations (tZFS). Dynamical decoupling (DD) measurements, using the Carr-  
17 Purcel sequence with  $\sim 140$  refocusing pulses, resolved the presence of two populations: one  
18 with a long phase relaxation time,  $T_{m,s}$ , and the other with a short one,  $T_{m,f}$ . The dominating  
19 mechanism for the slowly relaxing population is direct- $T_1$ .  $T_{m,s}$  showed no concentration  
20 dependence and was longer by a factor of about 2 from  $T_m$  for both complexes. We tentatively  
21 assign the increase in  $T_{m,s}$  to full suppression of the residual indirect  $T_1$ -induced NSD mechanism.  
22 For the fast relaxing population,  $T_{m,f}$  is shorter for Gd-TPMTA; therefore, we assign it to  
23 populations for which the tZFS mechanism dominates. Because of the relatively short  $T_1$  and the  
24 contribution of tZFS mechanism, protein deuteration does not significantly affect  $T_m$ .

25



1            1. Introduction

2            Distance measurements between two spin labels attached at specific sites in biomolecules,  
3            determined by pulse-dipolar EPR (PD-EPR) methods, have become standard tools in structural  
4            biology. The sensitivity of these measurements and the distance they can access depend on the  
5            phase memory time,  $T_m$ , of the spin labels used. Accordingly, understanding the decoherence  
6            mechanisms is essential for optimizing sample preparation conditions (concentrations, solvent  
7            composition, deuteration) and for spin-label design, thus reaching as long as possible  $T_m$ . In the  
8            case of solid-state EPR where the pulses applied cannot excite the entire width of the EPR  
9            spectrum, the spins are commonly divided into two types: Those excited and observed by the  
10            microwave pulse are referred to as the “A” spins, and the rest, termed “B” spins, are much more  
11            abundant. In general, at low temperatures, at which PD-EPR experiments are commonly carried  
12            out, there is no motion and the mechanisms contributing to decoherence for spin labels with  
13             $S=1/2$  are (Salikhov et al., 1981; Tyryshkin et al., 2012; Mitrikas, 2023; Wilson et al., 2023; Eaton  
14            and Eaton, 2000): (i) Direct spin-lattice ( $T_1$ ) relaxation mechanism of the A spins,  $T_{m,T_1}$ , which  
15            provides the highest limit  $T_m \leq 2T_1$ . (ii) Redistribution of resonance frequencies of dipole-  
16            coupled A spins due to mw pulses leads to instantaneous diffusion, ID. (iii) Coupling between A  
17            spins and nearby B spins leads to spectral diffusion, SD. The latter can result from  $T_1$  flips of the  
18            coupled B spins, referred to as indirect- $T_1$ , SD- $T_1$ , or energy-conserving pairwise B spin flip-flops,  
19            SD-ee. All these are concentration-dependent. (iv) Nuclear spin diffusion (NSD) arising from  
20            nuclear flip-flops caused by homonuclear couplings, which does not depend on the electron spin  
21            concentration but depends on the nuclei concentration. (v) Admixture of tunnel states of methyl  
22            groups into the electron spin mediated by the hyperfine coupling of methyl protons (Soetbeer et  
23            al., 2021a).

24            Gd(III) chelates are among the spin labels used for PD-EPR applications; they are beneficial for  
25            in-cell PD-EPR measurements because of their chemical stability and high sensitivity at high  
26            frequencies (> 34 GHz, Q- and W-band) owing to a narrow central transition and a relatively long  
27            phase memory time (Goldfarb, 2014; Giannoulis et al., 2021). Several studies have been  
28            dedicated to the dephasing mechanism of Gd(III) at low temperatures. Raitsimring et al  
29            (Raitsimring et al., 2014) explored the phase relaxation of Gd(III)-DOTA as a representative of  
30            Gd(III) spin labels in the temperature and concentration ranges typically used for W-band  
31            double electron-electron (DEER) measurements, which is the most widely applied PD-EPR



1 experiment.(Pannier et al., 2011) They found that in addition to the mechanisms of phase  
2 relaxation known for nitroxide-based spin labels listed above, Gd(III) spin labels are subjected to  
3 an additional phase relaxation mechanism that features an increase in the relaxation rate from  
4 the center to the periphery of the EPR spectrum. It was suggested that this mechanism is due to  
5 transient zero-field splitting (tZFS) fluctuations. This tZFS-induced phase relaxation mechanism  
6 becomes dominant (or at least significant) when all other phase relaxation mechanisms  
7 mentioned above are significantly suppressed by matrix (solvent) deuteration and low spin  
8 concentration.

9 A quantitative analysis of Gd(III) Hahn echo decay was recently reported at 240 GHz (Wilson et  
10 al., 2023). Two complexes, Gd-DOTA ( $D=700$  MHz) and Gd-PyMTA ( $D=1200$  MHz), were studied  
11 in  $D_2O$ /glycerol- $d_8$ .  $T_1$  and  $T_m$  were measured as a function of temperature and concentration. As  
12 expected  $T_1$  was found to be concentration-independent, whereas  $T_m$  was. Interestingly, the  
13 Hahn echo decay from which  $T_m$  was derived could be fitted by an exponential decay instead of  
14 the stretched exponent needed at Q-band (Soetbeer et al., 2021b). A careful analysis of the  
15 temperature and concentration dependence data and the associated  $T_1$  values gave the relative  
16 contributions of the various decoherence mechanisms. The concentration-independent  
17 mechanism was found to be the direct- $T_1$  mechanism and a concentration- and temperature-  
18 independent mechanism was assigned to weak coupling between electron spins and the  
19 presence of an ensemble of nuclear spins. As the solvent was fully deuterated, these could be  
20 protons on the Gd(III) complex. In this respect, it has been shown that while deuteration of  
21 nitroxides spin labels did not increase  $T_m$ , for trityl labels, it did (Soetbeer et al., 2021b).

22 Qualitative studies of several Gd(III) complexes, with axial parameters,  $D$ , of the ZFS in the range  
23 of 560-2000 MHz, investigated the effect of solvent deuteration at Q-band(Garbuio et al., 2015),  
24 and reported that in a protonated matrix,  $T_m$  is dominated by NSD. It was also suggested that in  
25 fully deuterated solvents, the phase relaxation is dominated by tZFS and perhaps ligand  
26 hyperfine-driven mechanism, but no quantitative analysis of the data was presented. The  
27 decoherence behavior of Gd(III) complexes was further investigated under dynamical  
28 decoupling (DD) conditions. DD is a control strategy to protect quantum states from  
29 decoherence, achieved by applying a sequence of carefully designed control pulses that  
30 counteract unwanted interactions with the environment, effectively "decoupling" the system  
31 from environmental noise.(Suter and Álvarez, 2016) CP (Carr-Purcell) and CPMG (Carr-Purcell-



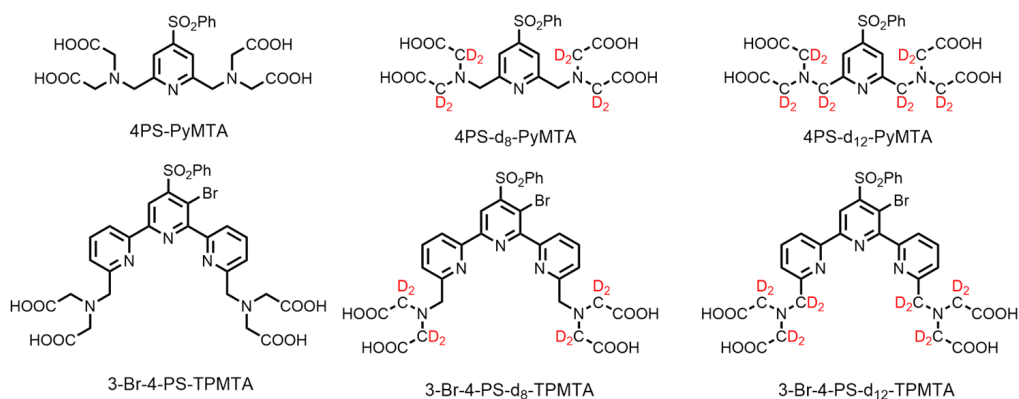
1 Meiboom-Gill) echo trains are such sequences. DD acts as a filter between the spin system and  
2 the environment, and the pulse spacing determines the characteristics of this filter. Short delays  
3 compared to the correlation time of the environmental fluctuations increase the coherence time  
4 of the system and typically, relaxation caused by electron-electron spectral diffusion and NSD  
5 can be suppressed (Soetbeer et al., 2021b; Soetbeer et al., 2018). Recent measurements on a  
6 single crystal of Gd(III) doped Y(trensol) carried out at X-band frequencies showed that CPMG  
7 with 120 refocusing pulses suppressed NSD efficiently and increased  $T_m$  considerably,  
8 depending on the transition probed and the crystal orientation (Hansen et al., 2024).

9 Three Gd(III) complexes with  $D$  values of 485-1861 MHz were studied at Q-band in protonated  
10 and deuterated solvent, H<sub>2</sub>O/glycerol and D<sub>2</sub>O/glycerol-d<sub>8</sub>, and a low concentration to suppress  
11 the ID and SD mechanisms (Soetbeer et al., 2021b). As expected, the solvent deuteration  
12 increased the decay time considerably, and the data could be well-fitted with a single stretched  
13 exponential decay function (SE model). Furthermore, for Gd-DOTA-M in deuterated solvents, DD  
14 (CP with up to 5 refocusing pulses) did not generate a significant increase in the decay time, and  
15 it was suggested that coherence losses of unknown origin, probably the ZFS-driven mechanism,  
16 which the DD cannot refocus, counteracted the decoupling efforts.(Soetbeer et al., 2021b)  
17 Interestingly, measurements of a protein singly spin-labeled with Gd-DOTA-M in a deuterated  
18 solvent increased the echo decay rate approximately threefold, as compared to the bare spin-  
19 label in the same solvent. This three-fold increase could be counter-acted by DD with 2-3 pulses,  
20 achieving overall longer coherence survival than any DD trace of the fully protonated sample  
21 (Soetbeer et al., 2021b). This showed that the protein's protons do affect phase relaxation. Thus,  
22 one would expect that deuteration of the protein should help reduce the decoherence.

23 In the present work, we explore whether deuteration of the Gd(III) chelate and the protein can  
24 further extend  $T_m$ , along with the effects of concentrations, temperature, and field position  
25 within the Gd(III) EPR spectrum. This is done for Hahn echo decay measurements, and the  
26 potential of DD for extending it further is also examined. We studied two Gd(III) spin-label  
27 complexes, PyMTA (Gd-PyMTA) and TPMTA (Gd-TPMTA) (**Fig. 1**), with different degrees of  
28 deuteration. These two complexes have very different  $D$  values (1200 vs ~4000 MHz). All  
29 measurements were carried out at W-band (95 GHz), and the complexes were dissolved in  
30 D<sub>2</sub>O/glycerol-d<sub>8</sub>, thus serving as a reference for the longest possible  $T_m$ . These are then  
31 compared to the phase relaxation of these labels when conjugated to a protein. We found that



1 the protons at a distance shorter than 5 Å from the Gd(III) do not contribute to NSD and that the  
2 protein's deuteration did not significantly prolong  $T_m$ . The primary mechanisms contributing to  
3 the phase relaxation in deuterated solvents and low concentrations are the direct  $T_1$  and tZFS  
4 mechanisms.

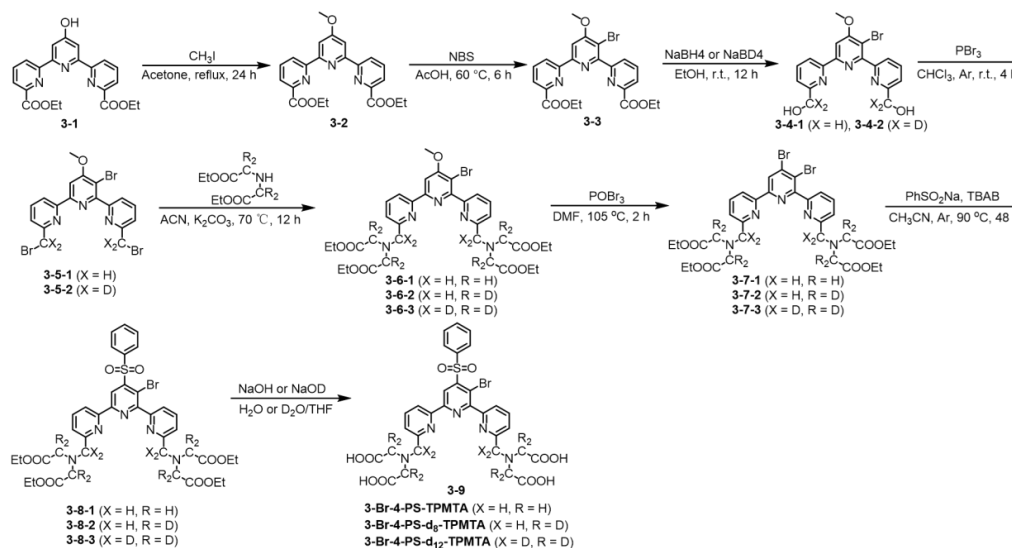


5  
6 **Figure 1.** Deuterated chelates for Gd(III) that can be further attached to cysteine residues in a  
7 protein for labeling.

## 8 1. Experimental

### 9 1.1 Synthesis of spin labels

10 The synthesis of spin tags, protein expression and labeling are described in detail in the  
11 Supporting Information. In brief, the 4PS-(d<sub>n</sub>)-PyMTA were synthesized according to reported  
12 procedure (Montgomery et al., 2017; Wang et al., 2019) (Li and Byrd, 2022) (Yang et al., 2015)  
13 and 3-Br-4-PS-(d<sub>n</sub>)-TPMTA tags were synthesized in the following 8 steps (Scheme 1). 1:  
14 Methylation of (3-1) with CH<sub>3</sub>I and K<sub>2</sub>CO<sub>3</sub> in acetone, purification via column chromatography  
15 (82% yield). 2: Bromination of (3-2) with N-Bromosuccinimide (NBS) in acetic acid at 60 °C, and  
16 chromatography purification (92% yield). 3: Reduction of (3-3) with NaBH<sub>4</sub>/NaBD<sub>4</sub> in ethanol,  
17 yielding a yellow solid. 4: Reaction of (3-4) with PBr<sub>3</sub> in CHCl<sub>3</sub>, followed by neutralization and  
18 extraction. 5: Substitution of (3-5) with diethyl iminodiacetate in acetonitrile at 70 °C, yielding a  
19 yellow solid. 6: Reaction of (3-6) with POBr<sub>3</sub> in DMF at 105 °C and purification. 7: Reaction of (3-  
20 7) with sodium benzene sulfinate and TBAB in acetonitrile at 90 °C. 8: Hydrolysis of (3-8) with  
21 NaOH/NaOD in THF/H<sub>2</sub>O, followed by acidification, resulting in (3-9) as a yellow solid. The  
22 synthesis of 4PS-5-Br-6PCA-(d<sub>n</sub>)-DO3A-Gd(III) is described in detail in the Supporting  
23 Information.



**Scheme 1.** Synthesis of 3-Br-4-PS-( $d_n$ )-TPMTA spin tags.

1

## 2 2.2 Protein purification, spin labeling, and EPR sample preparation

3 The D39C/E64C construct of ubiquitin (ub) was used in this study. The steps for deuterated  
4 protein expression were performed according to previous reports (Li and Byrd, 2022).

### 5 2.2.1 Protein labeling with 4PS-5-Br-6PCA-( $d_n$ )-DO3A-Gd(III).

6 0.2 mM 100  $\mu$ L purified protein ( $^1\text{H}$   $^{14}\text{N}$  ubi D39C/E64C or  $^2\text{H}$   $^{15}\text{N}$  ub D39C/E64C) was incubated  
7 with 0.4 mM tris(2-carboxyethyl)phosphine (TCEP) in 20 mM Tris-HCl at pH 8.5, and then treated  
8 with 10 equivalents of tags at 30  $^\circ\text{C}$  for 12 h. The reaction progress was monitored by ESI-Q-TOF  
9 mass spectrometry. The excess tag was removed using a PD-10 desalting column (GE Healthcare  
10 Biosciences). The ligation products were freeze-dried for subsequent experiments.

### 11 2.2.3 Protein labeling with 4PS-PyMTA or 3-Br-4PS-TPMTA.

12 The ligation of the target protein to 4PS-PyMTA was carried out according to the previous  
13 reports (Yang et al., 2019). 0.2 mM 100  $\mu$ L purified protein in 20 mM Tris-HCl at pH 8.5 was  
14 mixed with 0.4 mM TCEP, and then treated with 10 equivalents tags at 30  $^\circ\text{C}$  for 12 h. After the  
15 reaction was completed, the sample was filtered through PD-10 desalting column to remove the  
16 excess tag. The protein-PyMTA was mixed with 2.5 equivalents of  $\text{Gd}(\text{NO}_3)_3$  in a 20 mM MES  
17 buffer at pH 6.5. The excess of metal ion was removed using a Millipore concentrator (3 kDa  
18 cutoff). Similarly, 3-Br-4PS-TPMTA was conjugated to the target protein using the same



1 procedure, and the deuterated tags were ligated to the target protein the same as the non-  
2 deuterated tag.

3 For pulse EPR measurements, Gd-PyMTA and Gd-TPMTA solutions in the concentration range of  
4 0.03-0.2 mM were dissolved in 50:50 v/v D<sub>2</sub>O/glycerol-d<sub>8</sub>. The spin-labeled protein conjugates  
5 were lyophilized and redissolved in 15 mM HEPES-D<sub>2</sub>O buffer (pD 7.2) with 20% glycerol-d<sub>8</sub> (v:v).  
6 The final concentration of proteins was 50 μM estimated from the absorbance at 280 nm using a  
7 Nanodrop spectrophotometer (Thermo Science). For EPR measurements, solutions (ca. 3 μL)  
8 were transferred to quartz capillaries (0.6 ID × 0.84 OD mm) and sealed at one end with  
9 crytoseal.

### 10 2.3 *Spectroscopic measurements*

11 Pulsed EPR and ENDOR measurements were performed using two home-built W-band pulse EPR  
12 spectrometers equipped with cylindrical TE<sub>011</sub> cavities and Helmholtz radiofrequency (RF) coils  
13 (Gromov et al., 1999). The first spectrometer has a solenoid superconducting magnet  
14 (Cryomagnetics, Inc.), a 3 W pulsed microwave power amplifier (QPP95013530, Quinstar), and a  
15 pulsed 2 kW RF amplifier (BT02000-GammaS, TOMCO). The second spectrometer has a 0–5 T  
16 cryogen-free magnet with an integrated variable temperature unit and 300 mT sweep coil  
17 (J3678, Cryogenic Ltd.)(Feintuch et al., 2011), and is equipped with 2 W pulsed microwave  
18 power amplifier (QPP95023330-ZW1, Quinstar). All temperature and field dependencies of Gd -  
19 TPMTA- were carried out using the second spectrometer due to its wide temperature and  
20 magnetic field ranges.

21 Echo-detected EPR (ED-EPR) spectra were recorded employing the Hahn echo sequence ( $\pi/2$ - $\tau$ -  
22  $\pi$ - $\tau$ -echo) sequence and measuring the echo intensity as a function of the magnetic field. The  $\pi$   
23 pulse duration was 28-30 ns,  $\tau$ =500-600 ns, and a repetition time of 1 ms. Echo decays as a  
24 function of  $\tau$  were measured by setting the magnetic field to the maximum of the ED-EPR  
25 spectra with the experimental parameters described above. The Carr–Purcell (CP) based scheme  
26 experiments were carried out using the  $\pi/2 - (\tau/n - \pi - \tau/n)_n -$  echo sequence with a 2<sup>n</sup>-step  
27 phase cycling employed to filter out all additional echoes except the refocused ones (Soetbeer  
28 et al., 2018). For these experiments, n was from 1 to 5 with varying  $\tau$  for each value of n and  
29 measuring the intensity of the last echo as a function of  $\tau$ . Additionally, a full CP train  $\pi/2_x - (\tau -$   
30  $\pi_x - \tau -$  echo  $- \tau - \pi_x - \tau -$  echo)<sub>n</sub> (Mentink-Vigier et al., 2013) was applied with a two-step phase  
31 cycling on the first  $\pi/2$  pulse, with constant  $\tau$  in the range of 280 to 800 ns and the intensity of



1 each echo was measured, typically  $n \sim 140$ .  $T_1$  measurements were performed using the  
2 inversion recovery sequence,  $\pi - t_{\text{wait}} - \pi/2 - \tau - \pi - \tau - \text{echo}$ , with varying  $t_{\text{wait}}$ .  
3 Mims ENDOR spectra were recorded on the first spectrometer at 10-11K and a magnetic field  
4 corresponding to maximum echo intensity using the sequence  $\pi/2 - \tau - \pi/2 - T(\pi_{\text{RF}}) - \pi/2 - \tau - \text{echo} -$   
5  $[\tau_2 - \pi - \tau_2 - \text{echo}]_n$  with a four-step phase cycle and five CP echoes with  $\tau_2 = 600$  ns for detection,  
6 which was optimized for the best signal-to-noise ratio (Mentink-Vigier et al., 2013) The RF  
7 frequency was varied randomly (Epel et al., 2003) The experimental parameters for the Mims  
8 ENDOR spectra were  $T = 42 \mu\text{s}$ ,  $\tau$  varied from 280 ns to 600 ns. RF power was adjusted to yield the  
9 desired  $\pi_{\text{RF}}$  pulse length (40  $\mu\text{s}$ ), using a Rabi nutation sequence,  $\pi/2 - \tau - \pi/2 - T(t_{\text{RF}}) - \pi/2 - \tau - \text{echo}$ ,  
10 with a constant mixing time,  $T$ , of 100  $\mu\text{s}$  and varying RF pulse length,  $t_{\text{RF}}$ .

#### 11 2.4. Simulations of the ED-EPR spectra:

12 ED-EPR spectra were simulated using EasySpin program package (Stoll and Schweiger, 2006)  
13 using solid-state simulation function “pepper”. The distributions of ZFS parameters were  
14 considered using a built-in EasySpin functionality (DStrain parameter), and the Boltzmann  
15 thermal polarization of the electron spin levels at the W-band at the temperature of the  
16 experiment was taken into account. A Gaussian line shape with 0.1 mT width was used for  
17 simulations. To account for the difference in turning angles for different electron spin manifolds  
18 in a pulsed ED-EPR experiment, intensities of individual transitions  $|m_S\rangle \leftrightarrow |m_S + 1\rangle$  were  
19 renormalized according to  $\sin^3(\pi\alpha/2) \cdot \alpha^{-1}$  (Raitisring et al., 2013) where  
20  $\alpha = \sqrt{S(S+1) - m_S(m_S+1)} / \sqrt{S(S+1) + 0.25}$  and  $S = 7/2$ . This approach still does not  
21 consider the difference in phase memory times of different electron spin manifolds, which is  
22 minor for the short inter-pulse  $\tau$  delays used in the ED-EPR sequence (500–600 ns). The optimal  
23 values of the parameters were determined by non-linear least-squares fitting.

### 24 **3. Results and discussion**

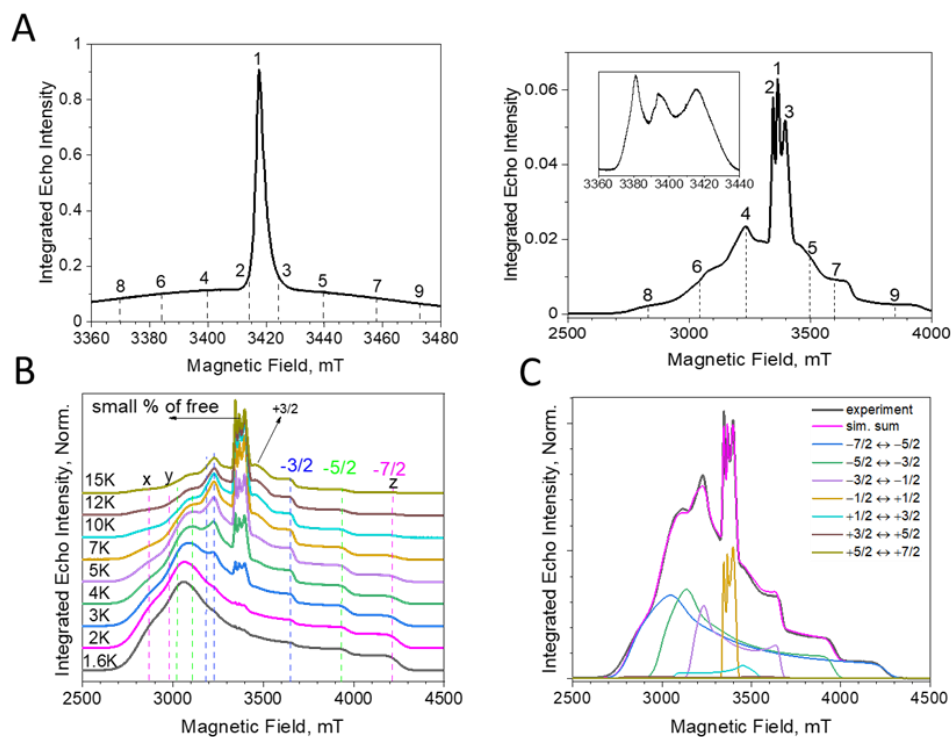
#### 25 3.1 Deuterated Gd(III) spin labels

##### 26 *3.1.1 ED-EPR and ENDOR spectra*

27 Before proceeding with the relaxation measurements, we carried out spectroscopic  
28 characterization of the samples. The W-band echo detected EPR (ED-EPR) spectra of Gd-PyMTA  
29 and Gd-TPMTA, recorded at 10K, are shown in **Fig. 2A,B**. The spectrum of Gd-PyMTA is typical  
30 for Gd(III) spin labels with a moderate ZFS ( $D = 1200$  MHz)<sup>27</sup> in frozen solutions where the  $m_S = -$



1  $1/2$  to  $m_s=1/2$  central transition (CT) dominates and appears as an intense peak superimposed  
2 on a broad featureless background arising from all other transitions. The unresolved broad  
3 background results from a large distribution in the ZFS parameters  $D$  and  $E$ . (Raitisring et al.,  
4 2005) The spectrum of Gd-TPMTA is unusual; the central transition has a fine structure, and the  
5 broad background on which it is superimposed has clear singularities. This indicates that the ZFS  
6 is considerably larger than for Gd-PyMTA and that the distributions of  $D$  and  $E$  are smaller. To  
7 ease the assignment of the various features of the spectrum, we recorded the spectrum at  
8 lower temperatures, where the contribution of the CT decreases and those of the low-lying  
9 transitions  $|-7/2\rangle \rightarrow |-5/2\rangle$  and  $|-5/2\rangle \rightarrow |-3/2\rangle$  increase. The spectra are presented in **Fig. 2C**  
10 with the annotation of the powder pattern's x, y, and z singularities corresponding to the various  
11 transitions. Simulations of the spectra presented in **Fig. 2D** gave  $D=4200$  MHz,  $\Delta D=390$  MHz,  
12  $E=440$  MHz, and  $\Delta E=370$  MHz. We attribute the larger ZFS values and the smaller distributions  
13 to TPMTA, offering optimal 9 coordination sites for Gd(III), holding it in a well-defined position  
14 as opposed to PyMTA, which has 7 coordination sites, and the other two are supplemented by  
15 water molecules.



1

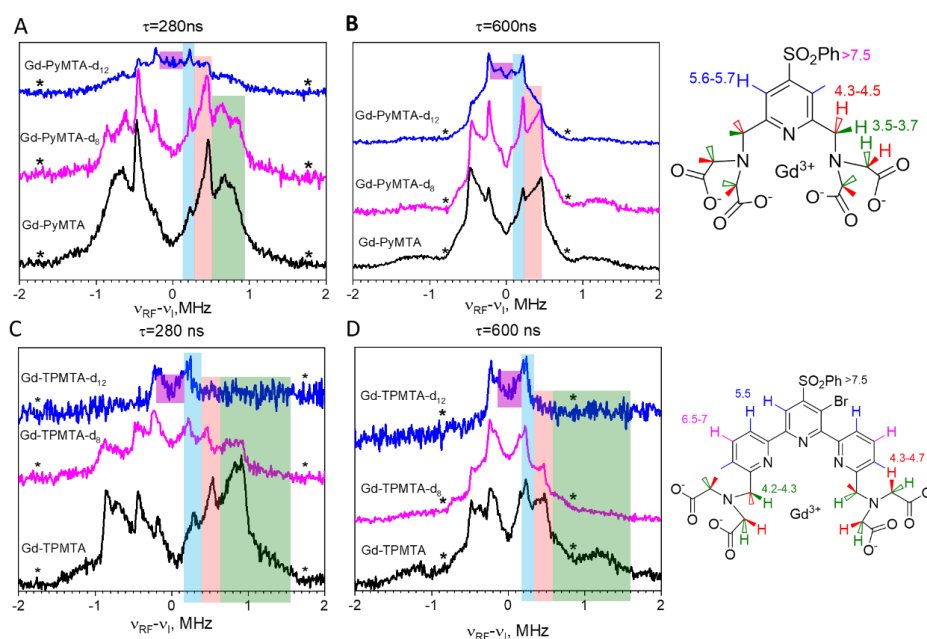
2 **Figure 2.** ED-EPR spectra (10 K) of Gd-PyMTA (A) and Gd-TPMTA (B). The central transition of  
3 Gd-TPMTA is shown in the insert on the right with an extended scale. The different numbers  
4 indicate positions at which relaxation measurements took place. C) Temperature-dependent ED-  
5 EPR spectra of Gd-TPMTA. The positions of the x,y,z singularities of the powder patterns of the  
6 various transitions are indicated. D) Simulations of the spectrum in (C) recorded at 5K, the  
7 simulation parameters are given in the text.

8 Next, we carried out W-band Mims ENDOR measurements to test the efficiency of the  
9 deuteration and determine the hyperfine couplings of the different protons, which are  
10 important for identifying their potential contributions to decoherence by NSD. **Fig. 3A,B**  
11 presents the spectra of Gd-PyMTA, Gd-PyMTA-d<sub>8</sub>, and Gd-PyMTA-d<sub>12</sub> measured with  $\tau=280$  ns to  
12 highlight the large <sup>1</sup>H couplings and  $\tau=600$  ns to highlight the small <sup>1</sup>H couplings.

13 For Gd-PyMTA-d<sub>12</sub> the spectrum is dominated by the protons on the pyridine ring, having a  
14 coupling  $a_{\perp}=440$  kHz, and the protons on the phenyl rings with  $a_{\perp}=140-170$  kHz, where  $a_{\perp}$  is the  
15 principal, perpendicular component of hyperfine tensor. A comparison of the spectra of the  
16 three Gd-PyMTA samples shows some residual methylene protons. The ENDOR spectra of Gd-  
17 TPMTA, Gd-TPMTA-d<sub>8</sub>, and Gd-TPMTA-d<sub>12</sub> are presented in **Fig. 4C,D**. In this case, the remaining



1 protons of Gd-TPMATA-d<sub>12</sub> are situated on three pyridine rings and are located 5.5 and 6.5-7 Å  
 2 away from the Gd(III) with a<sub>⊥</sub>=170-440 kHz. Here, the deuteration efficiency was higher than  
 3 that of Gd-PyMTA-d<sub>12</sub>, as we did not observe a significant contribution of residual methylene  
 4 protons. A summary of the hyperfine couplings of the various protons in Gd-PyMTA and Gd-  
 5 TPMATA is given in **Table S1**.



6

7 **Figure 3. (A,B)** Mims ENDOR spectra of Gd-PyMTA, Gd-PyMTA-d<sub>3</sub> and Gd-PyMTA-d<sub>12</sub> measured at  
 8 the CT with two  $\tau$  values (indicated on the figure). (C,D) Mims ENDOR spectra of Gd-TPMATA, Gd-  
 9 TPMATA-d<sub>3</sub>, and Gd-TPMATA-d<sub>12</sub>, measured at the low field peak of the CT, (3381 mT) with two  $\tau$   
 10 values (indicated in the figure). The assignment of the signals is given by the colored stripes  
 11 added to the spectra following the color code given on the complex structure given on the right.  
 12 The numbers next to the protons give the distances in Å extracted from the ENDOR doublets'  
 13 splitting. The asterisks mark the position of the blind spots.

### 14 3.1.2 Hahn echo decays

15 Hahn echo decays were measured for all samples and could be well-fitted with a single  
 16 stretched exponential decay function (SE model) (eq. 1) :

$$17 \quad y = A * \exp\left(-\frac{2\tau}{T_m}\right)^\beta \quad (1)$$

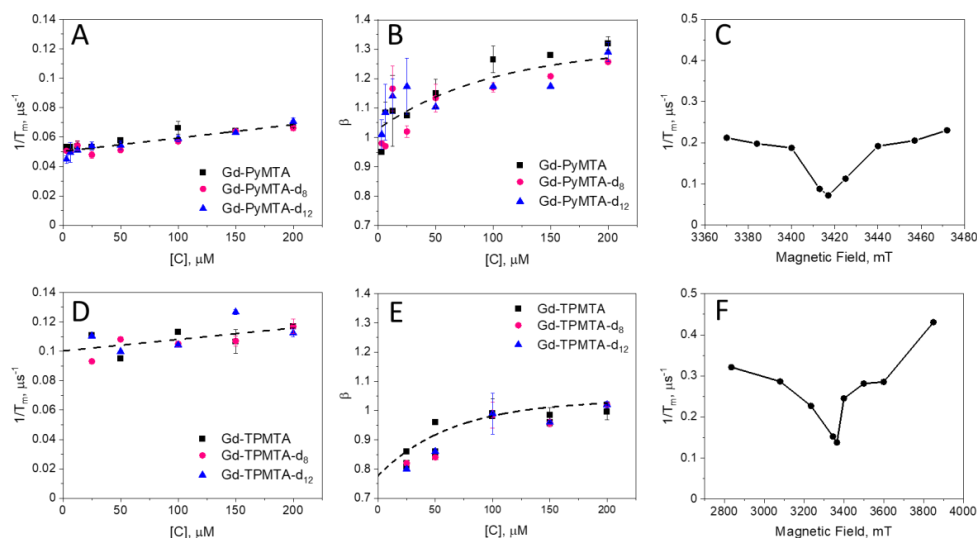


1 For Gd-PyMTA, measurements were carried out in the range of 3-200  $\mu\text{M}$ , and for Gd-TPMTA  
2 the range was 25-200  $\mu\text{M}$ ; concentrations lower than 25  $\mu\text{M}$  were not tested because of  
3 sensitivity limits owing to the broader EPR spectrum of Gd-TPMTA. A few examples of echo-  
4 decay data and their fits are shown in **Fig. S8**. The concentration dependence of  $1/T_m$  measured  
5 at 10 K on the CT for the PyMTA variants is given in **Fig. 4A**. We chose 10K because it is the  
6 optimal temperature for DEER measurements considering the populations of the CT and the  $T_m$   
7 temperature dependence. (Goldfarb, 2014) We did not detect any apparent effect of the degree  
8 of deuteration on  $T_m$  and  $\beta$ , both of which show a clear concentration dependence. This  
9 indicates that protons with hyperfine couplings in the range of 1-2 MHz (distance  $< 5 \text{ \AA}$ ) do not  
10 lead to decoherence as they may be within the nuclear spin diffusion barrier. (Wolfe, 1973)

11  $1/T_m$  of Gd-PyMTA is linearly dependent on concentration,  $[C]$ , and the intercept of  $0.05 \mu\text{s}^{-1}$   
12 gives  $T_m(0)=20 \mu\text{s}$ , this is  $T_m$  free of SD contributions. The dependence of  $\beta$  on  $[C]$  is not linear,  
13 reaching  $\beta=1$  for  $[C]\rightarrow 0$  (**Fig. 4B**). The dependence of  $1/T_m$  on the magnetic field within the EPR  
14 spectrum (10K and  $[C]=200 \mu\text{M}$ ), shown in **Fig. 4C**, reveals the same dependence as reported  
15 earlier (Raitsimring et al., 2014), where the central transition exhibits a longer  $T_m$ ; a characteristic  
16 of the tZFS mechanism (Raitsimring et al., 2014). The Hahn echo decay behavior of Gd-TPMTA,  
17 presented in **Fig. 4D-F**, was generally like that of Gd-PyMTA, disclosing no dependence on the  
18 deuteration levels. For Gd-TPMTA measurements, the concentration dependence  
19 measurements were carried out at three field positions (1,2,3, see **Fig. 2A**) within the CT, and  
20 the results of all three were practically the same; the data presented in **Fig. 4 D-F** corresponds to  
21 position 1. For Gd-TPMTA  $T_m(0)=10 \mu\text{s}$ , the value of  $\beta$  is lower than for Gd-PyMTA and  $\beta=0.8$  for  
22  $[C]\rightarrow 0$ . In general,  $\beta$  in the range of 1-2.5 suggests the presence of a fast dephasing process  
23 attributed to SD or NSD (Salikhov et al., 1981; Eaton and Eaton, 2000), whereas  $\beta < 1$  is typical of  
24 slow processes or is a signature of relaxation time distribution. (Salikhov et al., 1981)<sup>30</sup>  
25 Accordingly, we attribute the reduction in  $\beta$  with concentration to a reduction in the SD  
26 contribution, and the lower value of  $\beta$  at the low concentration limit of Gd-TPMTA is likely due  
27 to a larger, more extensive distribution of relaxation times. The latter arises from the larger ZFS  
28 and the significant contributions of transitions other than the CT at the CT field. We checked for  
29 the effect of ID for Gd-PyMTA with  $[C]=200 \mu\text{M}$  by measuring the echo decay as a function of  
30 the length of the second pulse and found a negligibly small contribution to  $1/T_m$  and  $\beta$  (see **Fig.**



1 **S9)**. Therefore, we conclude that the contribution of ID to the concentration dependence of  
2  $1/T_m$  is minimal.



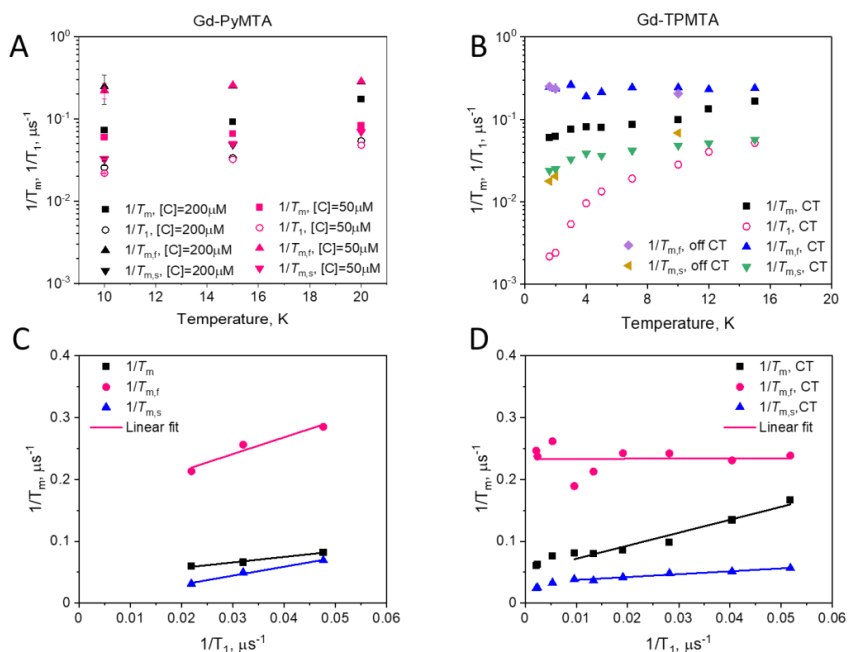
3

4 **Figure 4.** The dependence of  $1/T_m$  and  $\beta$ , measured at 10 K and the peak of the CT for the Gd-  
5 PyMTA variants (A,B) and Gd-TPMTA variants (D,E) measured at position 1 given in Fig. 2A. The  
6 dotted line in A and D is the linear fit with slopes of  $9.07 \times 10^{-5} \pm 8.2 \times 10^{-6}$  and  $7.79 \times 10^{-5} \pm 2.9 \times 10^{-5}$   
7  $(\mu\text{s}, \mu\text{M})^{-1}$  and intercepts of  $0.05 \pm 0.01$  and  $0.100 \pm 0.003 \mu\text{s}^{-1}$  for Gd-PyMTA and Gd-TPMTA  
8 respectively. The dotted lines in B and E were obtained with an exponential function  $y = y_0 +$   
9  $A_1 e^{-\frac{x}{T}}$  to guide the eye. The parameters used were  $y_0 = 1.3$ ,  $A = -0.28$ ,  $T = 100.8 \mu\text{s}$  and  $y_0 = 1.04$ ,  
10  $A = -0.26$ ,  $T = 64.5 \mu\text{s}$  for Gd-PyMTA and Gd-TPMTA respectively. (C, F) The field dependence of  
11  $1/T_m$  for 200  $\mu\text{M}$  Gd-PyMTA (C) and 200  $\mu\text{M}$  Gd-TPMTA (D), measured at 10 K.

12 Because the  $T_1$  values of Gd(III) are relatively short and can influence its phase relaxation, we  
13 carried out  $T_1$  and  $T_m$  measurements at different temperatures for Gd-PyMTA and Gd-TPMTA.  
14 We measured only the non-deuterated variants as we did not see any effect of the complex  
15 deuteration on the echo decays. The  $T_1$  values were determined from inversion recovery  
16 experiments and were analyzed using stretched exponents with values in the range of 0.7-0.8  
17 (see Fig. S10). Fig. 5A shows the temperature dependence of  $T_1$  and  $T_m$  of 200 and 50  $\mu\text{M}$  Gd-  
18 PyMTA; as expected  $T_1$  is concentration independent. For Gd-TPMTA a broader range of  
19 temperatures was accessed (1.6-15 K vs 10-20 K) and the results are given in Fig. 5B. For both  
20 complexes, we found that, unlike  $T_m$ ,  $T_1$  was independent of the field position within the EPR  
21 spectrum (Fig. S11); namely, it is the same for all Gd(III) EPR transitions. For Gd(III), we must  
22 consider that it is not only the relaxation times that change with temperature but also the



1 relative populations of the various transitions. Accordingly, changes in the levels' populations  
 2 can influence the  $T_m$  values measured at the CT. This effect is marginal for the temperature  
 3 range explored for Gd-PyMTA but can be significant for Gd-TPMTA below 7K.  
 4 To reveal the effect of  $T_1$  on  $T_m$ , we plotted  $1/T_m$  vs  $1/T_1$ , and the results are shown in **Figs. 5C-D**.  
 5 We observed a linear correlation for Gd-PyMTA (50  $\mu\text{M}$  and 200  $\mu\text{M}$ ). For Gd-TPMTA, where a  
 6 wider range of temperatures was probed, a linear correlation was observed only for the 5-15K;  
 7 below 5K  $1/T_m$  is fairly constant, indicating that the contribution of  $T_1$  to the phase relaxation is  
 8 no longer significant.



9

10 **Figure 5.** The temperature dependence of  $1/T_m$ , determined with Hahn echo and CP trains, and  
 11  $1/T_1$  for Gd-PyMTA (A) and Gd-TPMTA (B). The dependence of  $1/T_m$ , determined with Hahn echo  
 12 and CP trains on  $1/T_1$  for Gd-PyMTA (C) and Gd-TPMTA (D) along with the linear fit in the 6-20 K  
 13 range.

14

15 The slopes of  $1/T_m$  vs concentrations [C] for both complexes are the same within experimental  
 16 error (**Fig. 4**). This indicates that the contribution of  $1/T_{SD,ee}$  is negligible; otherwise a significant  
 17 difference would be expected because of the much broader EPR spectrum of Gd-TPMTA.  
 18 Therefore, we attribute the concentration dependence of  $1/T_m$  to the indirect- $T_1$ ,  $T_{SD,T1}$



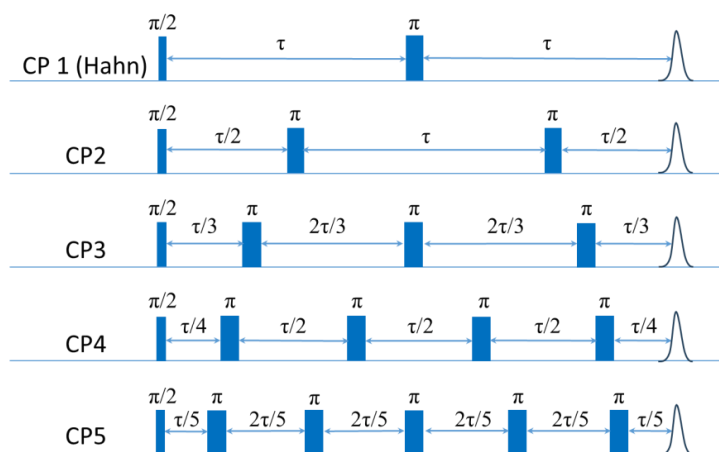
1 mechanism, which is lineshape independent. As the two complexes have similar  $T_1$  values,  
2 similar slopes are expected. We used the known expressions for  $T_{SD,T_1}$ , and  $T_{ID}$  to estimate their  
3 theoretical contributions (See **Fig. S12** and the associated text) for Gd-PyMTA. We found the  
4 predicted contribution of  $T_{ID}$  is negligible, consistent with our experimental results, and that the  
5  $T_{SD,T_1}$  calculated without any fitting parameters reproduces the experimental data reasonably  
6 (see **Fig. S12**), predicting a slope in the linear region of  $1.2 \times 10^{-4} \mu\text{s}^{-1}/\mu\text{M}$ , compared to the  
7 experimental slope  $0.9 \times 10^{-4} \mu\text{s}^{-1}/\mu\text{M}$ . The over-estimated concentration dependence can result  
8 from the non-exponential behavior of the echo decay and the inversion recovery, namely  $\beta \neq 1$ ,  
9 and the underestimation of  $T_1$  determined by the inversion recovery sequence. The  
10 contributions to  $T_m(0)$  can be from the direct- $T_1$  relaxation,  $T_{m,T_1}$ , residual NSD, and tZFS. As the  
11 contributions of spin diffusion, being either NSD or SD, to phase relaxation can be suppressed by  
12 DD, we proceeded with measurements of  $T_m$  using CP trains to further resolve the various  
13 contributions to phase relaxation.

### 14 3.1.3 CP with $n \leq 5$

15 To resolve the potential contribution of NSD induced by the very weakly coupled protons on the  
16 tags to decoherence, we followed the approach used by Jeschke and coworkers (Soetbeer et al.,  
17 2018), and measured the intensity of the last echo as a function of the interval between the  
18 pulses for CP trains with  $n=2-5$  refocusing pulses (see **Fig. 6**), while holding the time between the  
19 first  $\pi/2$  pulse and the last echo constant equal to  $2\tau$ . Interferences from overlapping stimulated  
20 echoes can be eliminated by phase cycling up to  $n=5$ ; beyond this, the phase cycle becomes too  
21 demanding (Soetbeer et al., 2018) (the phase cycles used are listed in **Table S2**). The resulting  
22 echo decays were analyzed using Eq.1 (examples of fits are shown in **Fig. S13**), and the data  
23 from the protonated spin labels are given in **Fig. 7A**, where we plotted  $1/T_m$  and  $\beta$  as a function  
24 of  $n$ , with  $n=1$  corresponding to the Hahn echo. We observed the same general behavior for 200  
25 and 25  $\mu\text{M}$  Gd-PyMTA; an initial significant decrease in  $1/T_m$  from  $n=1$  to  $n=2$ , followed by a mild  
26 change between  $n=2$  to  $n=4$  and leveling off at  $n=5$ .  $\beta$  exhibits a monotonic decrease from  $n=1$   
27 to  $n=3$  and levels off at  $n \geq 3$ , where it reaches a value of 1. Nevertheless, the systematically  
28 larger  $1/T_m$  for 200  $\mu\text{M}$  than that for 25  $\mu\text{M}$  and the reduction of the differences between with  
29  $n$ , shows that DD can suppress SD for the 200  $\mu\text{M}$  sample, though for  $n=5$  only partially. The  
30 behavior of Gd-TPMTA is similar but less pronounced;  $1/T_m$  decreases from  $n=1$  to  $n=2$  but then  
31 levels off and  $\beta$  levels off between  $n=3$  and  $n=4$ . We find the suppression of NSD contributions

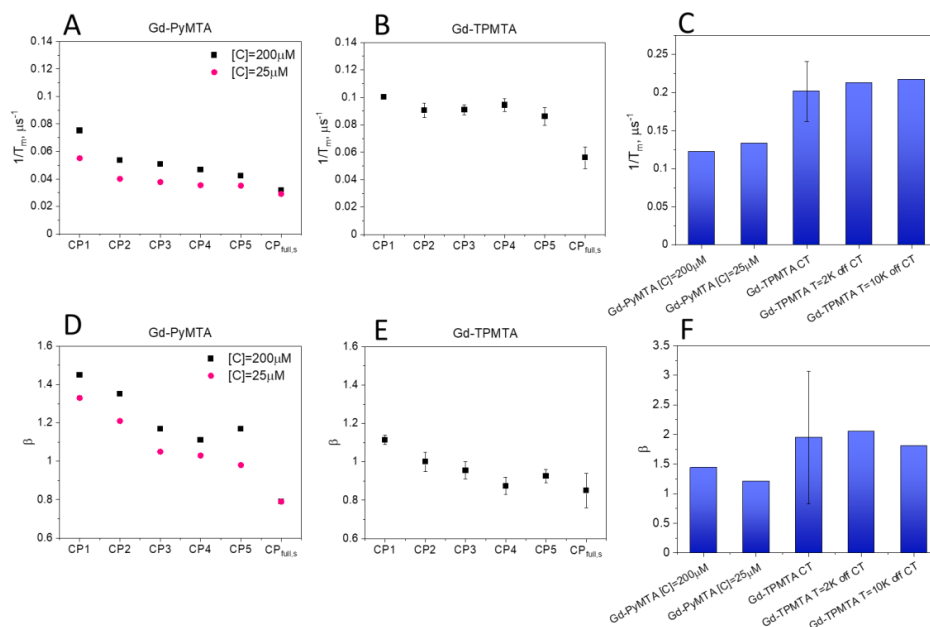


1 to be less likely because Gd-TPMTA has more weakly coupled protons on the label, and  
2 therefore, the effect should have been larger for Gd-TPMTA, but the opposite was observed.  
3 Such measurements, reported for Gd-DOTA-M in D<sub>2</sub>O:glycerol-d<sub>8</sub> (25 μM) at 10 K at Q-band,  
4 showed similar behavior, i. e. a mild decrease in 1/T<sub>m</sub> and β (Soetbeer et al., 2021b). T<sub>m</sub> reached  
5 40 μs for n=5 for Gd-DOTA-M, compared to 29 μs for Gd-PyMTA at W-band.



6

7 **Figure 6.** The CP sequences for n=1-5. n=1 corresponds to the Hahn echo.



1

2 **Figure 7.** Comparison of  $1/T_m$  measured at the CT and 10 K (A,B) and  $\beta$  (D,E), determined by CP  
 3 with  $n=1-5$  and those of the slow component in the full CP train for Gd-PyMTA (A,D) and Gd-  
 4 TPMTA (B,E). (C,F) Comparison of  $1/T_m$  of the fast component in the full CP train (C) and  $\beta$  (F) for  
 5 different complexes with different concentrations for Gd-PyMTA and Gd-TPMTA measured at  
 6 different field positions within the EPR spectrum.

### 7 3.1.4 Full CP train

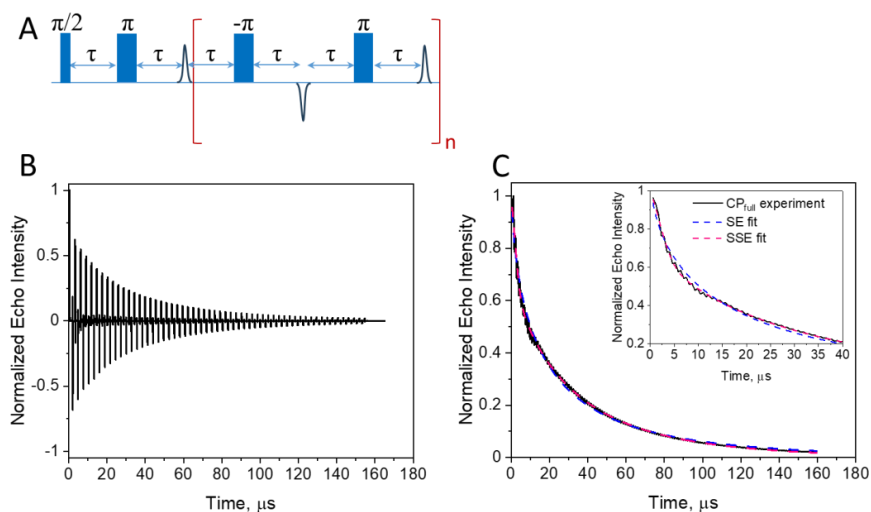
8 The very mild effect of CP with  $n=5$  on the phase relaxation of both complexes prompted us to  
 9 improve the effectiveness of the DD by applying a CP train pulse sequence with a constant inter-  
 10 pulse delay  $\tau$  (see **Fig. 8A**) and the shortest available on our spectrometer (290 ns), to suppress  
 11 potential contributions from fast processes to the phase relaxation. We refer to this as full CP  
 12 train. An example of the echo trains produced by this sequence is given **Fig. 8B**, and the plot of  
 13 the echo intensities as a function of time is presented in **Fig. 8C**. In this case, the data could not  
 14 be satisfactorily fitted with a single stretched exponent and a sum of two stretched exponents  
 15 (termed earlier as SSE (Soetbeer et al., 2018)) was used as follows:

$$16 \quad y = A * \exp\left(-\frac{t}{T_{m,f}}\right)^{\beta_f} + (1 - A) * \exp\left(-\frac{t}{T_{m,s}}\right)^{\beta_s} \quad (2)$$



1 where  $t$  is the time between the first  $\pi/2$  pulse and the observed echo, and the subscripts  $f$  and  
2  $s$  correspond to fast and slow processes.

3 As mentioned earlier, CP measurements with pulses that are not ideal because of their small  
4 bandwidth compared to the EPR spectral width produce echoes that are not pure refocused  
5 echoes but have contributions from stimulated echoes that decay with some combination of  $T_1$   
6 and spectral diffusion (Kurshev and Raitsimring, 1990; Mitrikas, 2023). To ensure that the  
7 observed SSE analysis is not a consequence of the contributions of such unwanted echoes, we  
8 performed a series of calculations presented in the SI (Figs. S14-S16). These show that the  
9 stimulated echo contribution leads to overestimation of  $T_m$  by no more than 20% and that a  
10 single stretched exponential function can fit the calculated echo intensities. To further ensure  
11 that the two observed components derived from the experimental results are not a  
12 consequence of artifacts in the applied pulse sequence, we carried out similar measurements on  
13 a nitroxide (MTSL) spin label in  $D_2O$ :glycerol- $d_8$  (25  $\mu M$ ), and the results are shown in Fig. S17. In  
14 this case, the echo train could be fitted well with only one stretched exponent. Therefore, we  
15 concluded that the two resolved populations are intrinsic to the Gd(III) complexes studied and  
16 are not a consequence of the stimulated echo contributions or experimental artifacts.



17

18 **Figure 8.** (A) The CP ( $n=137$ ,  $\tau=290$  ns) sequence applied and (B) the resulting echo train for Gd-  
19 PyMTA, 50  $\mu M$ , measured at 10 K and the maximum of the CT (C) The plot of the integrated echo  
20 intensity of the individual echoes as a function of time with the data fit using a single stretched  
21 exponential and a sum of two stretched exponentials. The inset shows an expanded part of the

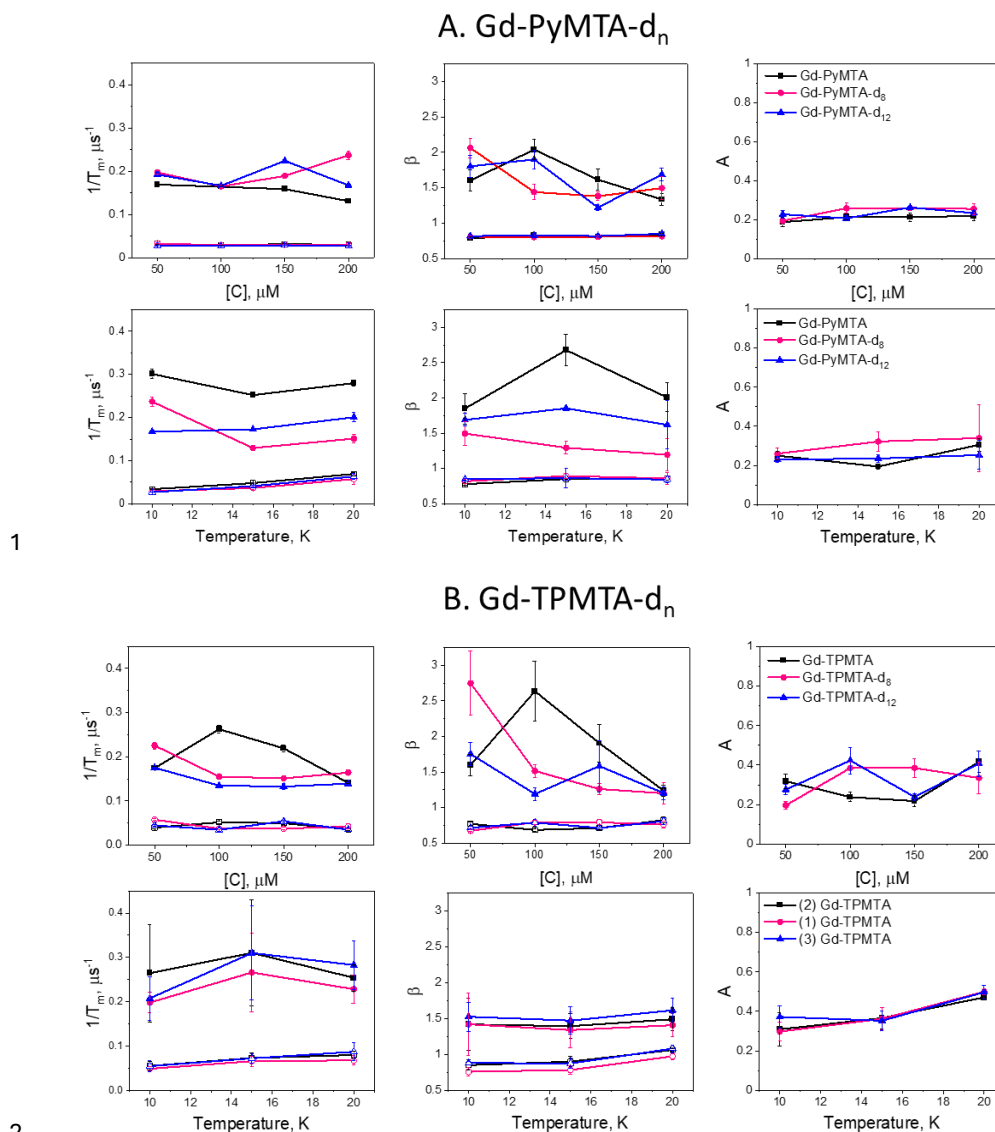


1 *trace, highlighting the fit differences. The fitting parameters were:  $T_m=32 \mu\text{s}$ ,  $\beta=0.58$ ,  $A=1.1$  for SE*  
2 *fit and  $T_{m,f}=3.3 \mu\text{s}$ ,  $\beta_f=1.85$ ,  $A_f=0.25$ ,  $T_{m,s}=29.6 \mu\text{s}$ ,  $\beta_s=0.78$ ,  $A=1.1$  for SSE fit, respectively.*

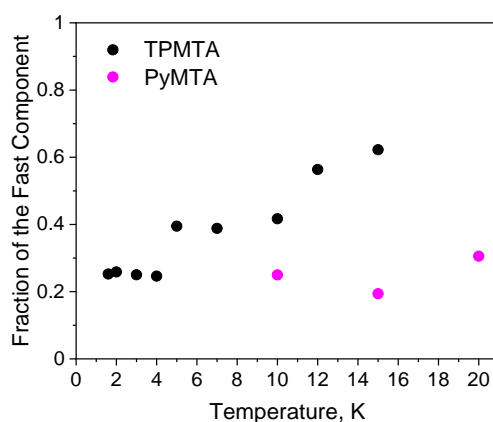
3

4 **Fig. 9** summarizes the dependence of the slow and fast CP decay rates,  $1/T_{m,s}$  and  $1/T_{m,f}$ , and  
5 the associated  $\beta_s$  and  $\beta_f$  on concentration and temperature for all Gd-PyMTA and Gd-TPMTA  
6 variants. The slow component of Gd-PyMTA, which has a contribution of 75-80%, is  
7 concentration and deuteration independent, and at 10 K  $T_m$  is 35  $\mu\text{s}$ , about twice as long as that  
8 measured by the Hahn echo decay (18  $\mu\text{s}$ ), well beyond the 20% expected overestimation. The  
9 same holds for  $\beta$ , which is reduced to about 0.75. For comparison with the values obtained with  
10  $n=1-5$  we added the data to **Fig. 7A,D**. Interestingly, while CP with  $n=5$  could not eliminate the  
11 concentration dependence, the entire train did ( $n \sim 140$ ). Here, the  $1/T_{m,s}$  value for 25 and 200  
12  $\mu\text{M}$  Gd-PyMTA coincided. We should bear in mind that the full CP train and CP  $n=2-5$  are  
13 different types of experiments; for the former, the number of  $\pi$  pulses and  $\tau$  are held constant  
14 and the recorded signal is the intensity of the occurring refocused echo after each  $\pi$  pulse, and  
15 for the latter the number of pulses is constant,  $\tau$  is varied and the intensity of the last echo is  
16 measured. This might be why full CP train refocuses the SD contributions better. There is an  
17 increase in  $1/T_{m,s}$  with temperature, whereas  $\beta_s$  and the relative population remain constant. For  
18 Gd-TPMTA, as for Gd-PyMTA, the slow component is not dependent on concentration nor  
19 deuteration level. Still, there is an increase of  $\beta_s$  and a decrease in its relative population with  
20 increasing temperatures. The values of  $1/T_{m,s}$  and  $\beta_s$  at 10 K are added to **Fig. 7B,E**  
21 for comparison with those obtained for  $n=1-5$ . The dependence of  $1/T_{m,s}$  on the temperature and  
22  $1/T_1$  for the two complexes are shown in **Fig. 5**.

23 For the fast component, the spread of the data points is quite large for all variants, and no  
24 systematic variation in concentration nor deuteration is observed. Here,  $T_{m,f}$  is 3-6  $\mu\text{s}$  and  $\beta_f=1.3-$   
25  $3$ ; no temperature or concentration dependence was detected within the experimental error. A  
26 comparison of the various values of  $1/T_{m,f}$  and  $\beta_f$  for different samples and temperatures is  
27 given in **Fig. 5C,F**. The relative contribution of the two components is fairly constant in the  
28 temperature range tested for Gd-PyMTA, whereas for Gd-TPMTA a significant increase in the  
29 contribution of the fast component with increasing temperature is observed in the range of 6-15  
30 K (**Fig. 10**).



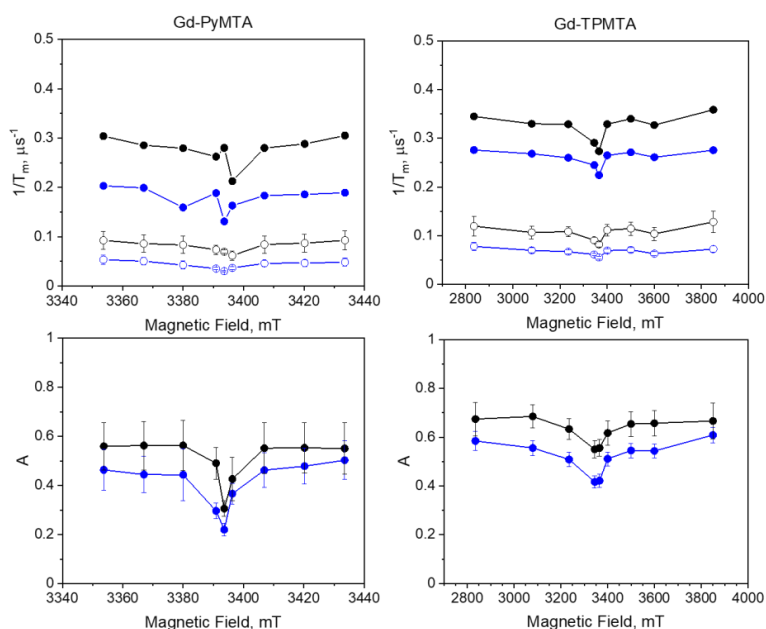
3 **Figure 9.** The dependence of the slow (open symbols) and fast (filled symbols) CP full train decay  
 4 rates, the associated stretched exponent and their relative population measured for: (A) The Gd-  
 5 PyMTA samples measured at the peak of the central transition as a function of concentration (10  
 6 K) and as a function of temperature for 200 μM. (B) The Gd-TPMTA samples measured at  
 7 position 1 in the central transition as a function of concentration (10 K) and as a function of  
 8 temperature for 200 μM Gd-TPMTA at field positions 1,2,3. The field positions are defined in Fig.  
 9 2.



1

2 **Figure 10.** The dependence of the relative contribution of the fast component, measured at the  
3 CT, as a function of temperature for Gd-PyMTA (magenta) and Gd-TPMTA (black).

4 We also investigated the field dependence of the decay rates of two components at two  
5 temperatures, 10 and 20 K (**Fig. 11**). For the Hahn echo, we observed a clear enhancement of  
6 the decay rate outside the CT; in contrast, the slow component showed a minimal change across  
7 the CT at both temperatures. Also, the difference between the CT and the other transitions was  
8 significantly weaker for the fast component than for the Hahn echo. Interestingly, the contrast  
9 between the CT and the other transitions is manifested in the two components' relative  
10 contributions. For both complexes, the contribution of the fast component is lower at the CT  
11 than outside the CT and the contribution of the fast component increases with temperature in  
12 all fields.



1

2 **Figure 11.** The field dependence of  $1/T_m$  for the slow and fast components at 10 and 20 K (top)  
3 and of the relative contribution of the fast component,  $A$  (see Eq. (2), (bottom)) for both  
4 complexes.

5

6 From the full CP train measurements, we conclude that (i) two populations of spins with  
7 different dominating phase relaxation mechanisms are observed for the two complexes. (ii) Any  
8 residual  $SD_{ee}$  and  $SD_{T_1}$  contributions are suppressed under the CP train conditions. (iii) We  
9 tentatively assign the dominating mechanism that governs the slow-relaxing population to the  
10 direct  $T_1$  mechanism and tZFS for the fast-relaxing population. (iv) The relative contribution of  
11 the tZFS mechanism is lower at the central transition than at the other transitions. (v) Gd-  
12 TPMTA, which has a significantly larger ZFS than Gd-PyMTA, has a larger population dominated  
13 by the tZFS, which is also temperature-dependent. The temperature dependence does not  
14 follow the relative intensity of the CT with temperature and, therefore, suggests that the tZFS  
15 fluctuations increase with temperature.

16

17



1 3.2. Influence of protein deuteration.

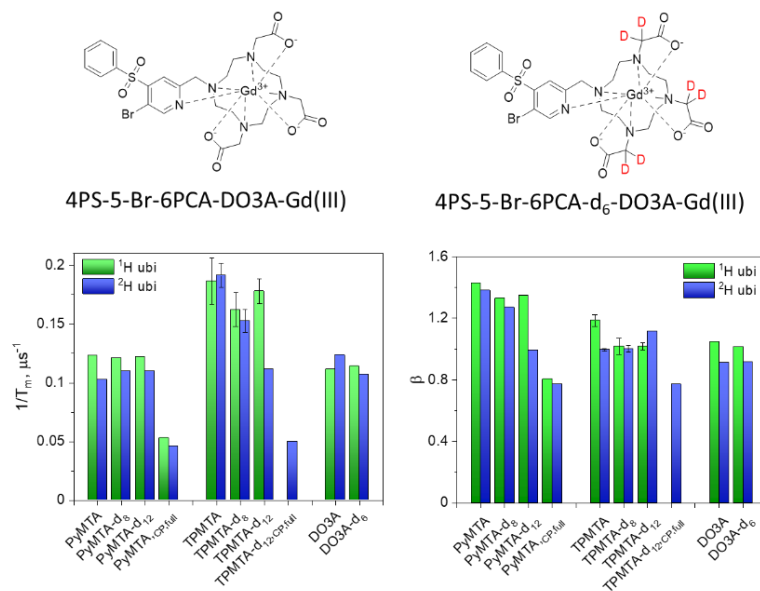
2 For nitroxide spin labels, protein deuteration increases  $T_m$ , by a factor of  $\sim 4$  (Ward et al., 2010;  
3 Schmidt et al., 2016). To see if Gd(III) spin labels experience the same effect, after exploring the  
4 phase relaxation behavior of the free Gd-PyMTA and Gd-TPMTA spin labels in deuterated  
5 solvents, we proceeded to examine their phase relaxation after their attachment to protonated  
6 and deuterated proteins in deuterated solvents. Ubiquitin D39C/E64C was labeled with Gd-  
7 PyMTA and Gd-TPMTA, producing doubly labeled proteins typically used for DEER applications.  
8 The concentrations were  $\sim 25 \mu\text{M}$  and  $\sim 50 \mu\text{M}$  for Gd-PyMTA and Gd-TPMTA labeled ubiquitin,  
9 respectively. The Hahn echo decays were fitted using Eq.1, as was done for the free labels  
10 (examples are shown in **Fig. S18**), and the results are summarized in **Fig. 12** for measurements  
11 on the CT at 10 K. The attachment to  $^1\text{H}$ -ubiquitin increased  $1/T_m$  by a factor of 2.4 for Gd-  
12 PyMTA and 1.8-1.9 for Gd-TPMTA, with no significant effect on the degree of label deuteration.  
13 While protein deuteration led to a slight decrease of  $1/T_m$  ( $\sim 10\%$ ) for Gd-PyMTA, for Gd-TPMTA  
14 labeled ubiquitin, a significant effect was noticed only for Gd-TPMTA- $d_{12}$ , almost reaching the  
15 value of the free label. The dependence of  $\beta$  on protein deuteration is insignificant for Gd-  
16 TPMTA. In contrast, for Gd-PyMTA, a gradual decrease with the increased degree of the label  
17 deuteration is observed for the deuterated protein, where for Gd-PyMTA- $d_{12}$  it reaches  $\beta=1$ , as  
18 for the free label. A small effect of the protein deuteration was also observed for the Gd-DO3A  
19 labeled ubiquitin ( $50 \mu\text{M}$ ) (**Fig. 12**). The low impact of protein deuteration on the Gd(III)  $T_m$   
20 values compared to nitroxide can be attributed to the Gd(III)'s much shorter  $T_1$ , which provides  
21 the upper limit to  $T_m$  ( $T_m \leq 2T_1$ ).

22 To further explore the origin of the significant reduction in the phase relaxation rate while  
23 bound to protein and the small effect of protein deuteration, we carried out full CP train  
24 measurements on the protonated and deuterated protein samples for Gd-PyMTA and Gd-  
25 TPMTA. Like the free labels, the data could not be fitted well with one stretched exponent, and  
26 a sum of two such exponents was needed, one with a fast decay and the other with a slow  
27 decay (**see Fig. S19**). The results for the population with the slow decay for protonated and  
28 deuterated ubiquitin with protonated Gd-PyMTA are shown in **Fig. 12**. The difference between  
29 the protonated and deuterated proteins was small. Same as in the case of the free label, we  
30 observed a reduction of about a factor of 2 in  $1/T_m$  for the slow population under CP train  
31 conditions, as compared to the value for Hahn echo. Interestingly,  $1/T_m$  in the free Gd-PyMTA in



1 a deuterated solvent is smaller by a factor of about two compared to the protein value. The  
2 same behavior was observed for Gd-TPMTA.

3 What is the source of the faster phase relaxation in the protein compared to the free complex?  
4 It cannot be attributed to the direct  $T_1$  mechanism because of the similar  $T_1$  values, 50.5  $\mu\text{s}$  for  
5 protein and 45.5  $\mu\text{s}$  for free complex. One possibility could be NSD from the non-deuterated  
6 HEPES molecules used as buffer, which results in 2.5% protons in the solvent. Another possibility  
7 could be the lower amount of glycerol in the protein samples (8:2 v/v vs 1:1 v/v for free Gd-  
8 PyMTA). To check this possibility, we prepared solutions of Gd-PyMTA in 15 mM HEPES in 8:2  
9 v/v vs 1:1 v/v  $\text{D}_2\text{O}$ /glycerol- $\text{d}_8$  and measured their Hahn-echo decays at 10K. The results, given in  
10 **Fig. S20**, show that the contribution of the protonated HEPES is small, but that of the lower  
11 amount of glycerol is significant. These two effects account only for about 80% of shorter  $T_m$  in  
12 the protein. An additional contribution can come from the fact that the proteins are doubly  
13 labeled, i.e., every Gd(III) center has a neighbor  $\sim 4.2$  nm away from it (see **Fig. S21**). Accordingly,  
14 its phase relaxation can be affected by indirect  $T_1$  due to the neighbor, which is concentration-  
15 independent. The relaxation of this neighbor is responsible for the Gd(III)-Gd(III) RIDME (The  
16 Relaxation-Induced Dipolar Modulation Enhancement) PD-EPR experiment, where it undergoes  
17 both single, double and triple quantum flips during the mixing time. (Razzaghi et al., 2014) In this  
18 case, mutual Gd(III) pair flip-flops can also induce relaxation. (Tyryshkin et al., 2012)



1

2 **Figure 12.** The structure of the Gd-DO3A label and the summary of the Hahn echo  $1/T_m$  and  $\beta$  of  
 3 ubiquitin labeled with Gd-PyMTA, Gd-TPMTA, and Gd-DO3A with various degrees of deuteration.  
 4 Gd-PyMTA, the results for the CPMG slow component have also been added.

5

## 6 **Conclusions.**

7 In this work, we explored the mechanisms responsible for the phase relaxation of Gd(III) spin  
 8 labels at 95 GHz, exploring whether deuteration of the label or the protein can extend the phase  
 9 relaxation. To resolve the relaxation mechanisms, we first studied the free label with different  
 10 degrees of deuterations in a deuterated solvent and examined both concentration and  
 11 temperature dependencies. We compared two labels having very different ZFSs, which helped  
 12 resolve various relaxation mechanisms.  $T_m$  was determined from both Hahn echo decay and CP  
 13 echo trains. Our conclusions are as follows:

- 14 1. Protons with hyperfine couplings in the 1-2 MHz range, situated at a distance  $<5 \text{ \AA}$ , do  
 15 not affect  $T_m$  and are located within the nuclear spin diffusion barrier.
- 16 2. In the range of 5-200  $\mu\text{M}$  the concentration dependence of the free tag is primarily  
 17 determined by the indirect  $T_1$ -induced mechanism.
- 18 3. At the limit of  $[C] \rightarrow 0$ , the contributions to  $T_m(0)$  can be residual NSD of the protons on  
 19 the pyridine rings with hyperfine couplings below 0.4 MHz, tZFS, and direct  $T_1$ . Since



1  $T_m(0)$  for Gd-TPMTA is shorter by a factor of about 2 and  $T_1$  values of both complexes  
2 are similar, we attribute the difference to the increased contribution of residual NSD or  
3 tZFS. Gd-TPMTA has 12 weakly coupled protons vs 7 for Gd-PyMTA, and its ZFS is  
4 significantly larger. The CP measurements with  $n=2-5$  had a more substantial suppression  
5 effect on  $T_m$  for Gd-PyMTA, suggesting that it originated from SD due to electron-  
6 electron interactions and that NSD was not suppressed under these conditions ( $n=5$ ),  
7 thus leaving tZFS and direct- $T_1$  as the mechanisms governing  $T_m(0)$ .

8 4. Full train CP measurements ( $n\sim 140$ ) resolved the presence of two populations: One with  
9 a slow phase relaxation and the other with a fast one. The dominating mechanism for  
10 the slow population is direct- $T_1$ . Its  $T_m$  showed no concentration dependence and was  
11 longer by a factor of about 2 relative to the Hahn echo decay for both complexes, yet  
12 keeping their relative values. We tentatively assign the decrease in  $1/T_{m,s}$  to full  
13 suppression of the residual indirect  $T_1$ -induced and NSD mechanism, made possible by  
14 the relatively short  $\tau=290$  ns used in the full train. This is supported by the more  
15 significant difference between  $n=5$  and the full train for Gd-TPMTA, which has more  
16 distant protons.

17 5. For the fast relaxing population,  $1/T_{m,f}$  is larger for Gd-TPMTA; therefore, we assign it to  
18 populations where the tZFS dominates, supported by its more extensive field  
19 dependence than  $1/T_{m,s}$ .

20 6. Because of the relatively short  $T_1$  and the contribution of the tZFS mechanism, protein  
21 deuteration does not significantly affect  $T_m$ . The shorter  $T_m$  for the doubly labeled  
22 proteins is attributed primarily to the lower glycerol amount in the sample and indirect-  
23  $T_1$  owing to the presence of a close-by Gd(III) neighbor.

24 The above shows that prolonging  $T_m$  would require increasing  $T_1$ , which can be achieved by  
25 lowering the temperature. However, this will be at the expense of the CT population, thus  
26 reducing sensitivity in DEER measurements. Another option is to reduce the spectrometer  
27 frequency, which again will cause broadening of the central transitions and impede sensitivity.  
28 Yet another way to increase  $T_m$  is to choose a label with a smaller ZFS (Ossadnik et al., 2025). A  
29 very small ZFS, however, introduces significant difficulties in analyzing DEER data for distances  
30 below 3 nm (Dalaloyan et al., 2015).

31



1 **Code and data availability:** All data reported herein and the EasySpin scripts for simulation of  
2 TPMTA tag ED-EPR spectrum can be accessed at <https://doi.org/10.5281/zenodo.15112854>

3 **Author contribution:** EE-investigation, visualization, writing – review and editing. XZ-  
4 investigation, visualization CC-investigation. YY-investigation. AB-formal analysis, methodology,  
5 writing – review and editing. GM -formal analysis, visualization, writing – review and editing XS-  
6 Conceptualization, funding acquisition, supervision, writing – review and editing. DG -  
7 Conceptualization, funding acquisition, supervision, writing – original draft preparation.

8 **Competing interests :** DG is a member of the executive editorial board of Magnetic Resonance.

#### 9 **Acknowledgments.**

10 The work was funded by the Joint NSFC (China) -ISF grant (No. 3559/21) and was made possible  
11 in part by support from the Helen and Martin Kimmel Institute for Magnetic Resonance  
12 Research and the historic generosity of the Harold Perlman Family (D. G.).

#### 13 **References**

- 14 Dalaloyan, A., Qi, M., Ruthstein, S., Vega, S., Godt, A., Feintuch, A., and Goldfarb, D.:  
15 Gd(III)-Gd(III) EPR distance measurements--the range of accessible distances and the  
16 impact of zero field splitting, *Phys. Chem. Chem. Phys.*, 17, 18464-18476,  
17 10.1039/c5cp02602d, 2015.
- 18 Eaton, S. S. and Eaton, G. R.: Relaxation Times of Organic Radicals and Transition Metal  
19 Ions, in: *Distance Measurements in Biological Systems by EPR*, edited by: Berliner, L. J.,  
20 Eaton, G. R., and Eaton, S. S., Springer US, Boston, MA, 29-154, 10.1007/0-306-47109-4\_2,  
21 2000.
- 22 Epel, B., Arieli, D., Baute, D., and Goldfarb, D.: Improving W-band pulsed ENDOR  
23 sensitivity-random acquisition and pulsed special TRIPLE, *J. Magn. Reson.*, 164, 78-83,  
24 10.1016/s1090-7807(03)00191-5, 2003.
- 25 Feintuch, A., Shimon, D., Hovav, Y., Banerjee, D., Kaminker, I., Lipkin, Y., Zibzener, K., Epel,  
26 B., Vega, S., and Goldfarb, D.: A Dynamic Nuclear Polarization spectrometer at 95 GHz/144  
27 MHz with EPR and NMR excitation and detection capabilities, *J. Magn. Reson.*, 209, 136-  
28 141, 10.1016/j.jmr.2010.12.010, 2011.
- 29 Garbuio, L., Zimmermann, K., Häussinger, D., and Yulikov, M.: Gd(III) complexes for  
30 electron–electron dipolar spectroscopy: Effects of deuteration, pH and zero field splitting,  
31 *J. Magn. Reson.*, 259, 163-173, <https://doi.org/10.1016/j.jmr.2015.08.009>, 2015.



- 1 Giannoulis, A., Ben-Ishay, Y., and Goldfarb, D.: Characteristics of Gd(III) spin labels for the  
2 study of protein conformations, *Meth. Enzymol.*, 651, 235-290,  
3 10.1016/bs.mie.2021.01.040, 2021.
- 4 Goldfarb, D.: Gd<sup>3+</sup> spin labeling for distance measurements by pulse EPR spectroscopy,  
5 *Phys.Chem.Chem.Phys.*, 16, 9685-9699, 10.1039/C3CP53822B, 2014.
- 6 Gromov, I., Krymov, V., Manikandan, P., Arieli, D., and Goldfarb, D.: A W-band pulsed  
7 ENDOR spectrometer: Setup and application to transition metal centers, *J. Magn. Reson.*,  
8 139, 8-17, 10.1006/jmre.1999.1762, 1999.
- 9 Hansen, S. H., Buch, C. D., Petersen, J. B., Rix, M., Ubach I Cervera, M., Strandfelt, A.,  
10 Winpenny, R. E. P., McInnes, E. J. L., and Piligkos, S.: Probing decoherence in molecular 4f  
11 qubits, *Chem. Sci.*, 15, 20328-20337, 10.1039/D4SC05304D, 2024.
- 12 Kurshev, V. V. and Raitsimring, A. M.: Carr-Purcell train in the conditions of partial  
13 excitation of magnetic resonance spectrum, *J. Magn. Reson.* (1969), 88, 126-129,  
14 [https://doi.org/10.1016/0022-2364\(90\)90113-N](https://doi.org/10.1016/0022-2364(90)90113-N), 1990.
- 15 Li, J. and Byrd, R. A.: A simple protocol for the production of highly deuterated proteins for  
16 biophysical studies, *J. Biol. Chem.*, 298, 102253,  
17 <https://doi.org/10.1016/j.jbc.2022.102253>, 2022.
- 18 Mentink-Vigier, F., Collauto, A., Feintuch, A., Kaminker, I., Le, V. T., and Goldfarb, D.:  
19 Increasing sensitivity of pulse EPR experiments using echo train detection schemes, *J.*  
20 *Magn. Reson.*, 236, 117-125, 10.1016/j.jmr.2013.08.012, 2013.
- 21 Mitrikas, G.: Long Electron Spin Coherence Times of Atomic Hydrogen Trapped in  
22 Silsesquioxane Cages, *J. Phys. Chem. Lett.*, 14, 9590-9595, 10.1021/acs.jpcllett.3c02626,  
23 2023.
- 24 Montgomery, J. R. D., Lancefield, C. S., Miles-Barrett, D. M., Ackermann, K., Bode, B. E.,  
25 Westwood, N. J., and Lebl, T.: Fractionation and DOSY NMR as Analytical Tools: From  
26 Model Polymers to a Technical Lignin, *ACS Omega*, 2, 8466-8474,  
27 10.1021/acsomega.7b01287, 2017.
- 28 Ossadnik, D., Qi, M., Voss, J., Keller, K., Yulikov, M., and Godt, A.: A Set of Three GdIII Spin  
29 Labels with Methanethiosulfonyl Groups for Bioconjugation Covering a Wide Range of EPR  
30 Line Widths, *The Journal of Organic Chemistry*, 90, 1847-1876, 10.1021/acs.joc.4c02441,  
31 2025.
- 32 Pannier, M., Veit, S., Godt, A., Jeschke, G., and Spiess, H. W.: Dead-time free measurement  
33 of dipole-dipole interactions between electron spins, *J. Magn. Reson.*, 213, 316-325,  
34 <https://doi.org/10.1016/j.jmr.2011.08.035>, 2011.
- 35 Raitsimring, A., Dalaloyan, A., Collauto, A., Feintuch, A., Meade, T., and Goldfarb, D.: Zero  
36 field splitting fluctuations induced phase relaxation of Gd<sup>3+</sup> in frozen solutions at cryogenic



- 1 temperatures, *J. Magn. Reson.*, 248, 71-80, <https://doi.org/10.1016/j.jmr.2014.09.012>,  
2 2014.
- 3 Raitsimring, A., Astashkin, A. V., Enemark, J. H., Kaminker, I., Goldfarb, D., Walter, E. D.,  
4 Song, Y., and Meade, T. J.: Optimization of Pulsed-DEER Measurements for Gd-Based  
5 Labels: Choice of Operational Frequencies, Pulse Durations and Positions, and  
6 Temperature, *Appl. Magn. Reson.*, 44, 649-670, 10.1007/s00723-012-0434-6, 2013.
- 7 Raitsimring, A. M., Astashkin, A. V., Poluektov, O. G., and Caravan, P.: High-field pulsed  
8 EPR and ENDOR of Gd<sup>3+</sup> complexes in glassy solutions, *Appl. Magn. Reson.*, 28, 281-295,  
9 10.1007/BF03166762, 2005.
- 10 Razzaghi, S., Qi, M., Nalepa, A. I., Godt, A., Jeschke, G., Savitsky, A., and Yulikov, M.: RIDME  
11 Spectroscopy with Gd(III) Centers, *J. Phys. Chem. Lett.*, 5, 3970-3975, 10.1021/jz502129t,  
12 2014.
- 13 Salikhov, K. M., Dzuba, S. A., and Raitsimring, A. M.: The theory of electron spin-echo signal  
14 decay resulting from dipole-dipole interactions between paramagnetic centers in solids, *J.*  
15 *Magn. Reson.* (1969), 42, 255-276, [https://doi.org/10.1016/0022-2364\(81\)90216-X](https://doi.org/10.1016/0022-2364(81)90216-X), 1981.
- 16 Schmidt, T., Wälti, M. A., Baber, J. L., Hustedt, E. J., and Clore, G. M.: Long Distance  
17 Measurements up to 160 Å in the GroEL Tetradecamer Using Q-Band DEER EPR  
18 Spectroscopy, *Angew. Chem. Intl. Ed.*, 55, 15905-15909,  
19 <https://doi.org/10.1002/anie.201609617>, 2016.
- 20 Soetbeer, J., Hülsmann, M., Godt, A., Polyhach, Y., and Jeschke, G.: Dynamical decoupling  
21 of nitroxides in o-terphenyl: a study of temperature, deuteration and concentration effects,  
22 *Phys.Chem.Chem.Phys.*, 20, 1615-1628, 10.1039/C7CP07074H, 2018.
- 23 Soetbeer, J., Ibáñez, L. F., Berkson, Z., Polyhach, Y., and Jeschke, G.: Regularized  
24 dynamical decoupling noise spectroscopy – a decoherence descriptor for radicals in glassy  
25 matrices, *Phys.Chem.Chem.Phys.*, 23, 21664-21676, 10.1039/D1CP03103A, 2021a.
- 26 Soetbeer, J., Millen, M., Zouboulis, K., Hülsmann, M., Godt, A., Polyhach, Y., and Jeschke,  
27 G.: Dynamical decoupling in water-glycerol glasses: a comparison of nitroxides, trityl  
28 radicals and gadolinium complexes, *Phys.Chem.Chem.Phys.*, 23, 5352-5369,  
29 10.1039/D1CP00055A, 2021b.
- 30 Stoll, S. and Schweiger, A.: EasySpin, a comprehensive software package for spectral  
31 simulation and analysis in EPR, *J. Magn. Reson.*, 178, 42-55,  
32 <https://doi.org/10.1016/j.jmr.2005.08.013>, 2006.
- 33 Suter, D. and Álvarez, G. A.: Colloquium: Protecting quantum information against  
34 environmental noise, *Rev.Mod. Phys.*, 88, 041001, 10.1103/RevModPhys.88.041001, 2016.



- 1 Tyryshkin, A. M., Tojo, S., Morton, J. J. L., Riemann, H., Abrosimov, N. V., Becker, P., Pohl,  
2 H.-J., Schenkel, T., Thewalt, M. L. W., Itoh, K. M., and Lyon, S. A.: Electron spin coherence  
3 exceeding seconds in high-purity silicon, *Nat. Mat.*, 11, 143-147, 10.1038/nmat3182, 2012.
  
- 4 Wang, G., Liang, X., Chen, L., Gao, Q., Wang, J.-G., Zhang, P., Peng, Q., and Xu, S.: Iridium-  
5 Catalyzed Distal Hydroboration of Aliphatic Internal Alkenes, *Angew. Chem. Intl. Ed.*, 58,  
6 8187-8191, <https://doi.org/10.1002/anie.201902464>, 2019.
  
- 7 Ward, R., Bowman, A., Sozudogru, E., El-Mkami, H., Owen-Hughes, T., and Norman, D. G.:  
8 EPR distance measurements in deuterated proteins, *J. Magn. Reson.*, 207, 164-167,  
9 <https://doi.org/10.1016/j.jmr.2010.08.002>, 2010.
  
- 10 Wilson, C. B., Qi, M., Han, S., and Sherwin, M. S.: Gadolinium Spin Decoherence  
11 Mechanisms at High Magnetic Fields, *J. Phys. Chem. Lett.*, 14, 10578-10584,  
12 10.1021/acs.jpcllett.3c01847, 2023.
  
- 13 Wolfe, J. P.: Direct Observation of a Nuclear Spin Diffusion Barrier, *Phys. Rev. Lett.*, 31, 907-  
14 910, 10.1103/PhysRevLett.31.907, 1973.
  
- 15 Yang, Y., Wang, J.-T., Pei, Y.-Y., and Su, X.-C.: Site-specific tagging proteins via a rigid,  
16 stable and short thiolether tether for paramagnetic spectroscopic analysis, *Chem. Comm.*,  
17 51, 2824-2827, 10.1039/C4CC08493D, 2015.
  
- 18 Yang, Y., Yang, F., Li, X.-Y., Su, X.-C., and Goldfarb, D.: In-Cell EPR Distance Measurements  
19 on Ubiquitin Labeled with a Rigid PyMTA-Gd(III) Tag, *J. Phys.Chem.B*, 123, 1050-1059,  
20 10.1021/acs.jpcb.8b11442, 2019.
  
- 21